Delayed Embryonic Development and Impaired Cell Growth and Survival in *Actg1* Null Mice

Tina M. Bunnell and James M. Ervasti*

Department of Biochemistry, Molecular Biology and Biophysics, University of Minnesota, Minneapolis, Minnesota

Actins are among the most highly expressed proteins in eukaryotes and play a central role in nearly all aspects of cell biology. While the intricate process of development undoubtedly requires a properly regulated actin cytoskeleton, little is known about the contributions of different actin isoforms during embryogenesis. Of the six actin isoforms, only the two cytoplasmic actins, β_{cyto}- and γ_{cyto}-actin, are ubiquitously expressed. We found that γ_{cyto}-actin null ($Actg1^{-/-}$) mice were fully viable during embryonic development, but most died within 48 h of birth due to respiratory failure and cannibalization by the parents. While no morphogenetic defects were identified, $Actg1^{-/-}$ mice exhibited stunted growth during embryonic and postnatal development as well as delayed cardiac outflow tract formation that resolved by birth. Using primary mouse embryonic fibroblasts, we confirm that γ_{cyto}-actin is not required for cell migration. The $Actg1^{-/-}$ cells, however, exhibited growth impairment and reduced cell viability, defects which perhaps contribute to the stunted growth and developmental delays observed in $Actg1^{-/-}$ embryos. Since the total amount of actin protein was maintained in $Actg1^{-/-}$ cells, our data suggests a distinct requirement for γ_{cyto}-actin in cell growth and survival. © 2010 Wiley-Liss, Inc.

Key Words: actin isoforms, cell migration, cell viability, murine embryonic development

Introduction

Actins are a major component of the cytoskeleton and play fundamental roles in most cellular processes, including muscle contraction, cell motility, cell division, cell signaling, establishment of cell polarity and maintenance of cell shape. In higher eukaryotes there are six different actin isoforms, each encoded by distinct genes: four "muscle" actins predominately expressed in striated (α_{sk} and α_{ca}) and smooth (α_{sm} and γ_{sm}) muscle and two cytoplasmic "nonmuscle" actins (β_{cyto} and γ_{cyto}) which are ubiquitously expressed [Rubenstein, 1990]. The actin family of proteins is highly conserved, with no two isoforms differing by more than 7% of its primary amino acid sequence. Incredibly, β_{cyto}- and γ_{cyto}-actin differ at only 4 out of 375 amino acids and these small sequence differences are conserved from birds to mammals.

It has been hypothesized that the β_{cyto}- and γ_{cyto}-actin isoforms confer unique functions in certain tissues and cell types. In support of this hypothesis, β_{cyto}- and γ_{cyto}-actin mRNA and protein segregate to distinct intracellular compartments in a variety of cell types [Yao et al., 1995; Bassell et al., 1998; Furness et al., 2005; Dugina et al., 2009]. Furthermore, siRNA-induced silencing revealed β_{cyto}- and γ_{cyto}-actin as essential genes in cultured mammalian cells [Harborth et al., 2001], suggesting non-redundant roles for the two non-muscle actin isoforms. In addition, hypomorphic β_{cyto}-actin mice are embryonic lethal [Shawlot et al., 1998; Shmerling et al., 2005], indicating that β_{cyto}-actin plays an essential role during embryonic development.

During animal development, a properly regulated actin cytoskeleton is required to generate the protrusive and contractile forces necessary for morphogenetic processes. Disruption of the actin cytoskeleton, either through perturbations in actin-binding proteins or through the use of actin-targeting drugs, leads to morphogenetic defects in several organisms, including worms, flies and mice [Jacinto and Baum, 2003; Copp et al., 2003; Marston and Goldstein, 2006]. In addition, actin is important for completing cell division, generating cell polarity, and maintaining cell shape, all processes critical for proper embryonic development. Despite the well-recognized roles for actin during development, little is know about the individual contributions from the different actin isoforms. Indeed, β_{cyto}- and γ_{cyto}-actin isoforms exhibit differential expression patterns during development [McHugh et al., 1991], suggesting that each isoform performs specific and perhaps unique functions.

We previously generated $Actg1^{-/-}$ mice and showed that γ_{cyto}-actin is not essential for viability, suggesting that other actin isoforms can at least partially compensate for γ_{cyto}-actin

*Address correspondence to: Dr. James M. Ervasti, Biochemistry, Molecular Biology and Biophysics, University of Minnesota, 6-155 Jackson Hall, 321 Church Street SE, Minneapolis, MN 55455, USA.
E-mail: jervasti@umn.edu

during embryonic development [Belyantseva et al., 2009]. However, only one-third of the expected number of $Actg1^{-/-}$ mice were found at the time of weaning [Belyantseva et al., 2009]. Therefore, we sought to characterize the embryonic and postnatal development of $Actg1^{-/-}$ mice to help identify processes that specifically require the γ_{cyto}-actin isoform during development. Surprisingly, $Actg1^{-/-}$ embryos were found at the expected Mendelian ratio throughout development and did not exhibit any gross developmental abnormalities. The observed lethality of $Actg1^{-/-}$ mice occurred within the first 48 h of birth, most likely resulting from respiratory distress. This lethality could be explained by the mild developmental delays or stunted growth observed in $Actg1^{-/-}$ embryos. Moreover, $Actg1^{-/-}$ mouse embryonic fibroblasts (MEFs) exhibited growth deficiencies due to reduced cell survival. Together, these data indicate that γ_{cyto}-actin is not essential for embryonic development; however, γ_{cyto}-actin does confer advantages for growth and survival.

Materials and Methods

Animals

Generation of $Actg1^{+/-}$ mice was described previously [Belyantseva et al., 2009]. Animals were housed and treated in accordance with the standards set by the University of Minnesota Institutional Animal Care and Use Committee. Timed matings were carried out by housing a single $Actg1^{+/-}$ male with one to two $Actg1^{+/-}$ estrous females overnight. Vaginal plugs were checked the following morning as an indication that copulation had occurred, and male and females separated. The day a plug was detected was considered E0.5 of development. At the designated embryonic age, pregnant females were euthanized and embryos liberated from the uterine muscle and deciduum. For each embryo, gross morphology was observed, crown-rump measurements taken and yolk sac or tail tissue recovered for genotype assessment. Genotypic analysis was performed using PCR methods described previously [Sonnemann et al., 2006]. Pregnant females were observed giving birth and newborn pups were monitored. Within 3 h of birth, lungs were dissected and examined.

Histology and Immunohistochemistry

Embryonic and postnatal tissue was fixed in Bouin's fluid for 2–24 h, depending on the size of the tissue, and stored in 70% ethanol at 4°C. Tissue was subsequently paraffin embedded and sectioned at 6 μm. Hematoxylin and eosin staining of tissue sections was carried out as described [Kaufman, 1992]. Immunohistochemistry was performed using the standard Avidin-Biotin Complex technique. Tissue sections were deparaffinized in xylenes, rehydrated through a series of graded ethanol and endogenous peroxidase activity quenched with 1.0% H_2O_2. Tissue was blocked with 2.5% goat serum and incubated with a polyclonal antibody to surfactant protein B (abcam, ab40876) for 1.5 h at room temperature. Sections were then incubated with a biotinylated secondary

antibody (Vector Laboratories, BA1000), followed by incubation with the avidin:biotinylated enzyme complex (R.T.U. Vectastain Elite ABC Reagent, Vector Laboratories, PK7100). Immune signal was detected by exposure to the peroxidase substrate 3,3′-diaminobenzidine. Tissue sections were counterstained with hematoxylin. Histological analyses were carried out on serial sections from at least three different animals for each genotype/age described.

Isolation and Culture of Primary MEFs

Primary MEF cultures were established from E13.5 embryos. Embryos were dissected in sterile PBS and the brain, heart, liver and other visceral organs removed. The carcass was then finely minced with a razorblade and incubated in 3.0 ml of 0.25% trypsin-EDTA at 4°C overnight. Once the embryonic genotypes were determined, the minced tissue was incubated in a 37°C water bath for 30 minutes to activate the trypsin. After vigorous pipetting to break up the digested tissue, the cell suspension from each embryo was plated on two 10-cm tissue culture dishes with 10 ml of MEF culture medium (Dulbecco's Modified Eagle's Medium supplemented with 10% fetal bovine serum, 50 units/ml Penicillin, 50 μg/ml Streptomycin and 100 μM nonessential amino acids). The following day, cell monolayers were rinsed with sterile PBS and fresh MEF culture medium added. Cells were split at approximately 90% confluency using 0.05% trypsin-EDTA and all analyses were carried out before the fourth passage. Cells were incubated in a humidified 37°C, 5% CO_2 incubator.

Analysis of Actin Composition and Migration in MEFs

Cell monolayers from nearly confluent 10-cm plates were washed twice with ice-cold PBS. After addition of 300 μl of ice-cold lysis buffer (50 mM Tris-HCl, pH 8.0, 150 mM NaCl, 1.0% NP-40, 0.02 mM PMSF, 0.05 μg/ml leupeptin, 5 mM EGTA), cells were collected by scraping and incubated on ice for 10 minutes. Cellular debris was removed by centrifugation and the protein concentration of the supernatant was assayed with the Bio-Rad *DC* Protein Assay Kit. Equal amounts of total protein were separated by SDS/PAGE and immunoblotted with the indicated antibodies (pan-actin, C4 (Seven Hills Bioreagents); γ_{cyto}-actin, mAb 2-4 (Sonnemann et al. 2006); β_{cyto}-actin, AC15 (Sigma); α_{smooth}-actin, 1A4 (Sigma); $\alpha_{sarcomeric}$-actin, 5C5 (Sigma)). The ratio of G-actin versus F-actin was determined with the G-actin/F-actin In Vivo Assay Kit (Cytoskeleton, BK037) based on the manufacturer's protocol. Briefly, cells were lysed in F-actin stabilization buffer and cell lysates centrifuged at $100,000 \times g$ to separate the F-actin from G-actin pool. The F-actin pellet was resuspended to the same volume as the supernatant and equal amount of samples loaded to each lane and analyzed by Western blotting using a pan-actin antibody (C4, Seven Hills Bioreagents). For the positive control sample, 1 μM phalloidin was added to the lysis buffer and incubated with wild-type cells. For both actin isoform
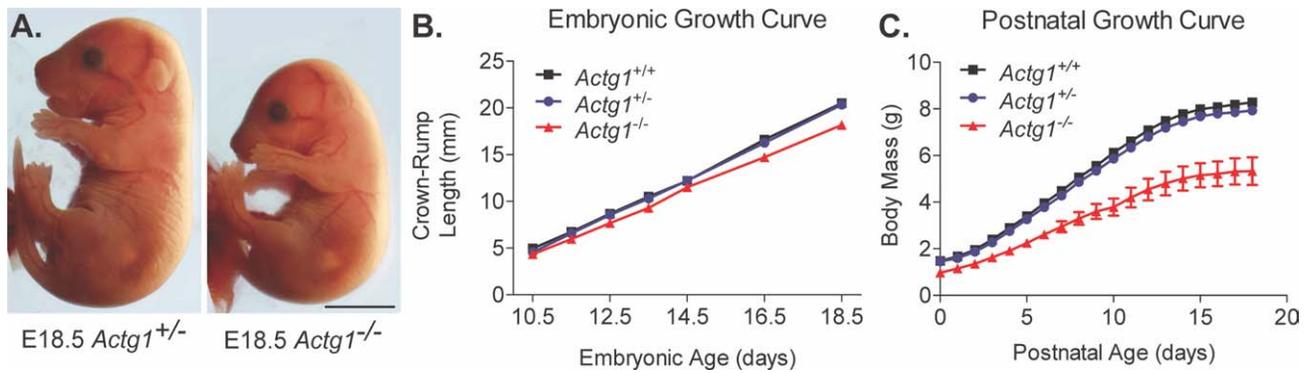
Fig. 1. Stunted growth in *Actg1*⁻/⁻ mice. A: Shown are representative images of E18.5 *Actg1*⁺/⁻ and *Actg1*⁻/⁻ embryos. Scale bar: 5 mm. **B**: Crown-rump length and **C**: body mass measurements during embryonic and postnatal development. *Actg1*⁻/⁻ mice were significantly (one-way ANOVA, $P < 0.05$) smaller than *Actg1*⁺/⁺ and *Actg1*⁺/⁻ controls from E11.5 onward. $n \geq 4$ for each genotype/timepoint; error bars represent s.e.m.

composition and G/F-actin ratio analyses, fluorescently labeled secondary antibodies were detected and quantified from at least three separate experiments using an Odyssey infrared scanner and software (Li-Cor Biosciences, Lincoln, NE).

Rates of MEF cell migration were assessed using a standard scratch wound-healing assay. Cells were plated on glass-bottom dishes (MatTek Corp.) and allowed to grow to confluency. Using a yellow pipette tip, a "wound" or scratch was made across the bottom of the dish. Cell monolayers were subsequently rinsed with sterile PBS and fresh media, containing 25 mM HEPES to stabilize the pH, added to the cells. For optical clarity, a glass coverslip was used to seal the dish, creating a self-contained sterile environment. Time-lapse video of migrating cells was captured overnight at 10 min intervals using differential interference contrast (DIC) imaging on a Delta Vision personalDV (Applied Precision, Inc., Issaquah, Washington) with a 40× (NA 1.35) oil objective using softWoRx 3.7.1 software. The cells were maintained at 37°C by an environmental chamber enclosing the microscope. ImageJ 1.43 software was used to measure wound area in the first frame and also in the frame just before the edges of the wound first meet (approximately the 20th frame). The rate of migration was calculated as the change in wound area divided by the change in time.

Analysis of Cell Growth in MEFs

Cell size and viability were determined using the Vi-CELL Series Cell Viability Analyzer (Beckman Coulter). Cell monolayers were rinsed with PBS, harvested by trypsinization and resuspended in 1.0 ml of PBS before automated analysis by the Vi-CELL. Between 200 and 3000 cells were analyzed per sample. For the growth curve, equal numbers (10^5) of passage 1 MEFs were plated in each well of 6-well plates and counted every 24 h in duplicate using the Vi-CELL. Cell cycle analysis was carried out using flow cytometry to determine total DNA concentration per cell after ethanol fixation and staining with a 20 µg/ml propidium iodide (PI) solution containing 200 µg/ml ribonuclease A. The PI

fluorescent signal was collected on a BD Biosciences (San Jose, CA) FACSCalibur and cell cycle phases estimated using FlowJo software (Tree Star).

Apoptosis was detected using a FITC Annexin V Apoptosis Detection Kit (BD Pharmingen). Cells were cultured for 48 h, after which culture media was collected and cells trypsinized and counted. Cells were resuspended to the same concentration in Binding Buffer and equal volumes incubated with FITC-Annexin V and Propidium Iodide for 15 minutes at room temperature in the dark. Samples were subsequently diluted with Binding Buffer and analyzed by flow cytometry within an hour. 5 µM camptothecin was added to a plate of wild-type cells 6 h before harvesting to serve as a positive control. Compensation between FL1 and FL3 was carried out using FlowJo software (Tree Star) and data collected from singly stained samples. The Vi-Cell and FACS-Calibur instruments were used at the University of Minnesota's Masonic Cancer Center Flow Cytometry Core Facility.

Results

Stunted Growth and Delayed Cardiac Development in *Actg1*⁻/⁻ Mice

Timed matings were established between *Actg1* heterozygous pairs and resulting *Actg1*⁻/⁻ embryos examined. *Actg1*⁻/⁻ embryos were morphologically similar to their wild-type counterparts throughout development (Fig. 1a). However, they were 11% smaller in size, as measured by crown-rump length, from embryonic day (E) 10.5 to E18.5 (Fig. 1b). *Actg1*⁻/⁻ mice remained smaller in size during the first 3 weeks of postnatal development (Fig. 1c) and into adulthood [Belyantseva et al., 2009].

Histological analysis of the developing embryo revealed a delay in the development of the cardiac outflow tract in *Actg1*⁻/⁻ embryos. During cardiac development, the proximal portion of the outflow cushions fuse and muscularize, eventually walling the aorta into the left ventricle and completing the formation of the ventricular septum [Anderson et al.,
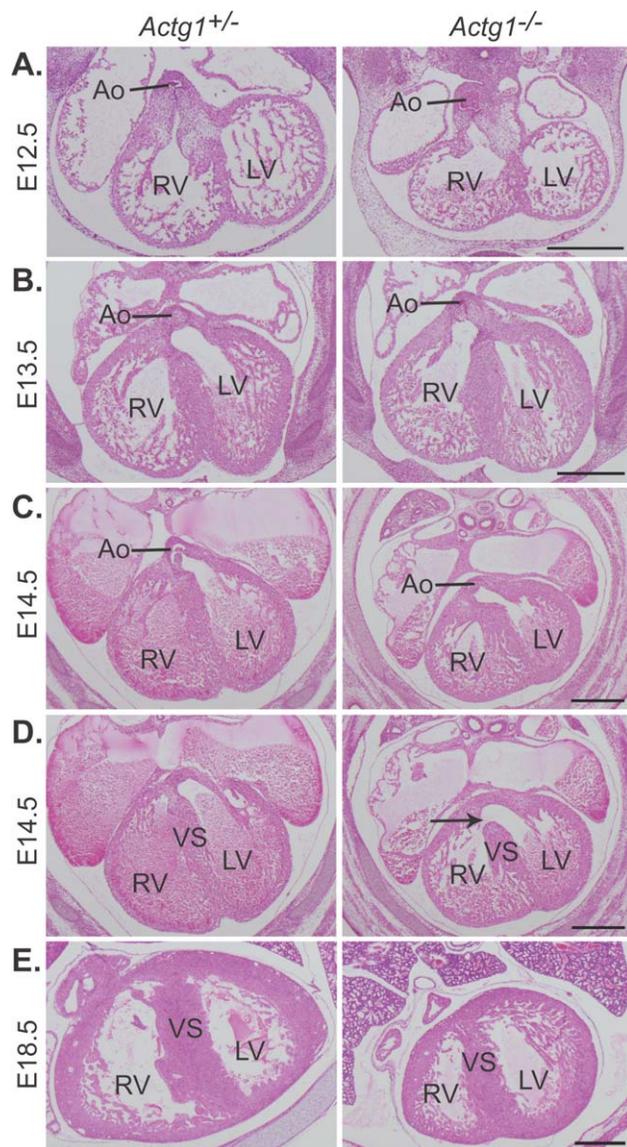
Fig. 2. Delayed development of the cardiac outflow tract in *Actg1*$^{-/-}$ **embryos.** Shown are typical hematoxylin and eosin stained transverse sections through the embryonic heart. **A**: At E12.5 the aorta was observed to be in communication with the right ventricle in both *Actg1*$^{+/-}$ and *Actg1*$^{-/-}$ embryos. **B**: By E13.5 the aorta was observed in exclusive communication with the left ventricle in *Actg1*$^{+/-}$ embryos but remained in communication with the right ventricle in all six *Actg1*$^{-/-}$ embryos examined. **C**: By E14.5, however, the aorta had been walled into the left ventricle in six out of seven *Actg1*$^{-/-}$ embryos. **D**: At E14.5 in *Actg1*$^{+/-}$ embryos, but not in the seven *Actg1*$^{-/-}$ embryos examined (arrow), the ventricular septum was completely formed along the entire anterior–posterior axis. **E**: By E18.5 the ventricular septum had fully developed in all *Actg1*$^{-/-}$ embryos. Scale bars: 500 µm. Ao, aorta; LV, left ventricle; RV, right ventricle; VS, ventricular septum.

2003]. In wild-type embryos the aorta was observed to be exclusively in communication with the left ventricle by E13.5, however, in *Actg1*$^{-/-}$ embryos this was not observed until E14.5 of development (Figs. 2b and 2c). Furthermore, in wild-type embryos but not *Actg1*$^{-/-}$ embryos, the ventricular septum was fully formed along the entire anterior–poste-

rior axis by E14.5 (Fig. 2d). The ventricular septum was completely formed by E18.5 in *Actg1*$^{-/-}$ embryos, indicating a developmental delay rather than a failure of cardiac outflow tract formation (Fig. 2e).

Postnatal Lethality in *Actg1*$^{-/-}$ Mice

We previously measured sub-Mendelian ratios of *Actg1*$^{-/-}$ mice at weaning [Belyantseva et al., 2009]. To determine the time point of lethality, timed matings were established and genotype ratios determined at all stages of development. *Actg1*$^{-/-}$ embryos were found at the expected frequency up through E18.5 of development (Table I), indicating that γ_{cyto}-actin is not required for embryonic viability. However, within 24 h following birth the observed frequency of *Actg1*$^{-/-}$ mice was significantly less than the expected Mendelian ratio (Table I). These data reveal that the observed lethality in *Actg1*$^{-/-}$ mice occurs postnatally.

Direct observation of litters born from timed matings of heterozygotes revealed that some *Actg1*$^{-/-}$ mice presented with respiratory distress at birth. Histological analysis of the developing lung did not indicate any gross morphological defects of *Actg1*$^{-/-}$ embryos (Fig. 3a). Furthermore, the expression of surfactant protein B, a marker of lung development, was comparable between *Actg1*$^{+/-}$ and *Actg1*$^{-/-}$ mice at E18.5 (Fig. 3a). At the time of birth, however, some *Actg1*$^{-/-}$ mice experienced difficulty breathing, which correlated with variations in the extent of saccular inflation in the lung (Fig. 3b). These data suggest that the increased postnatal lethality of *Actg1*$^{-/-}$ mice was primarily due to respiratory distress, which in turn led to maternal cannibalism of the affected pups.

Characterization of *Actg1*$^{-/-}$ Mouse Embryonic Fibroblasts

In order to assess cellular behavior in the absence of γ_{cyto}-actin, primary MEFs were generated from *Actg1*$^{+/+}$, *Actg1*$^{+/-}$ and *Actg1*$^{-/-}$ E13.5 embryos. We confirmed that *Actg1*$^{-/-}$ MEFs completely lacked expression of γ_{cyto}-actin protein and showed that MEFs carrying only one wild-type copy of the *Actg1* gene had reduced expression of γ_{cyto}-actin (Figs. 4a and 4b). Despite the absence or reduction of γ_{cyto}-actin expression, total actin expression levels were not different across all genotypes (Figs. 4a and 4b). Total actin levels were

Table I. Partial Postnatal Lethality in *Actg1*$^{-/-}$ Mice

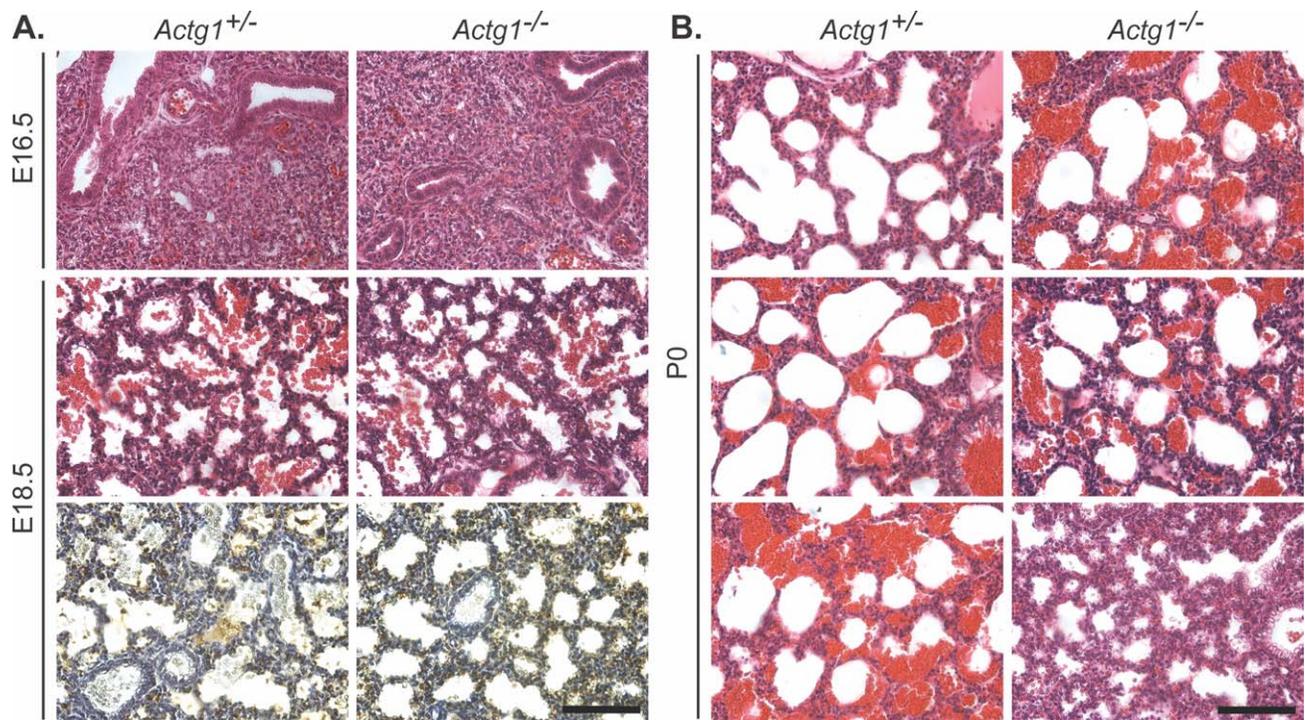| Age	n	*Actg1*$^{+/+}$	*Actg1*$^{+/-}$	*Actg1*$^{-/-}$
E10.5–14.5	434	23%	54%	23%
E16.5	86	30%	50%	20%
E18.5	113	22%	58%	20%
P0[a]	153	27%	63%	10%
P1[a]	139	27%	68%	5%

[a]$P < 0.05$, χ^2 analysis.

Fig. 3. Partially penetrant respiratory failure observed in *Actg1*⁻/⁻ newborns. Shown are representative transverse sections of the developing lung. **A**: Hematoxylin and eosin staining of *Actg1*⁻/⁻ lungs at E16.5 (top row) and E18.5 (middle row) revealed comparable morphology to wild-type. Immunohistochemistry using an antibody to surfactant protein B as a marker of lung development showed no differences in expression between *Actg1*⁺/⁻ and *Actg1*⁻/⁻ lungs at E18.5 (bottom row). **B**: In *Actg1*⁻/⁻ lungs at P0 the extent of saccular inflation was variable and corresponds with observed variations in ability to breath at the time of birth. Scale bars: 100 μm.
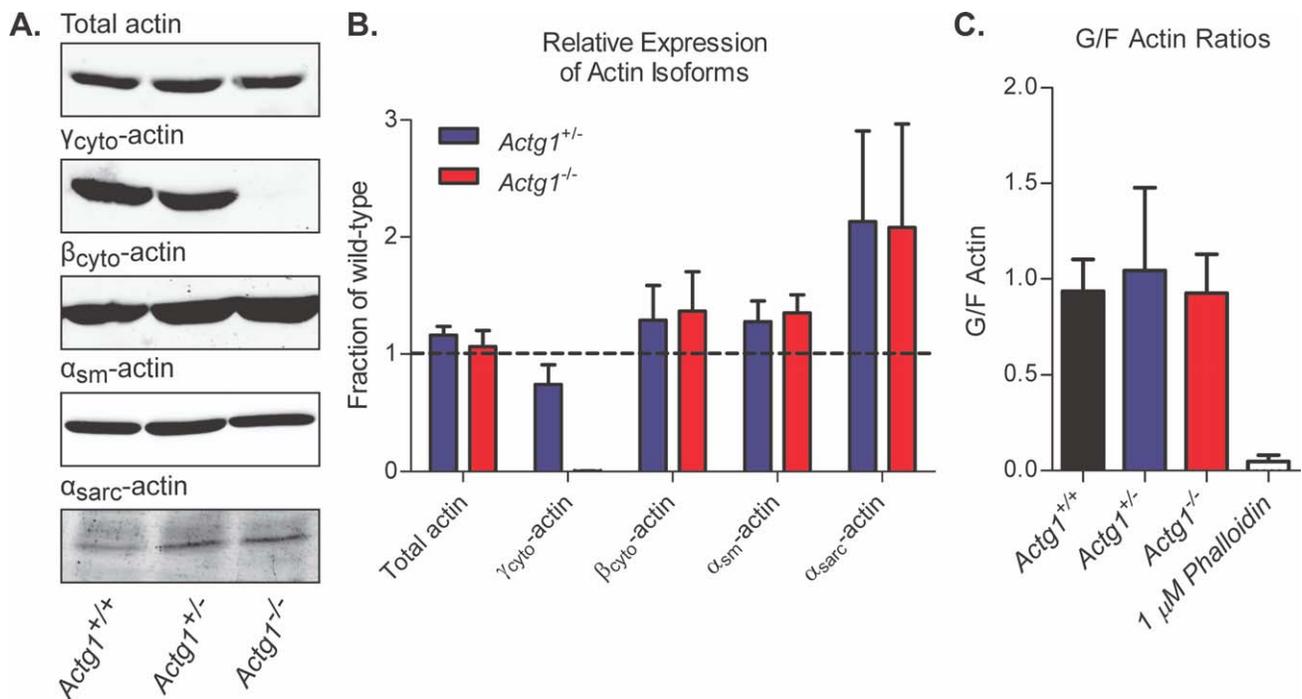

Fig. 4. Altered actin isoform expression with no change in levels of total actin in *Actg1*⁻/⁻ MEFs. A: Representative immunoblots of cell lysates from *Actg1*⁺/⁺, *Actg1*⁺/⁻ and *Actg1*⁻/⁻ MEFs probed with actin isoform specific antibodies. **B**: Protein levels were quantified and are expressed relative to wild-type levels ($n \geq 3$, mean ± s.e.m.). **C**: Quantification of G- to F-actin ratios in *Actg1*⁺/⁺, *Actg1*⁺/⁻ and *Actg1*⁻/⁻ MEFs ($n \geq 3$, mean ± s.e.m.).
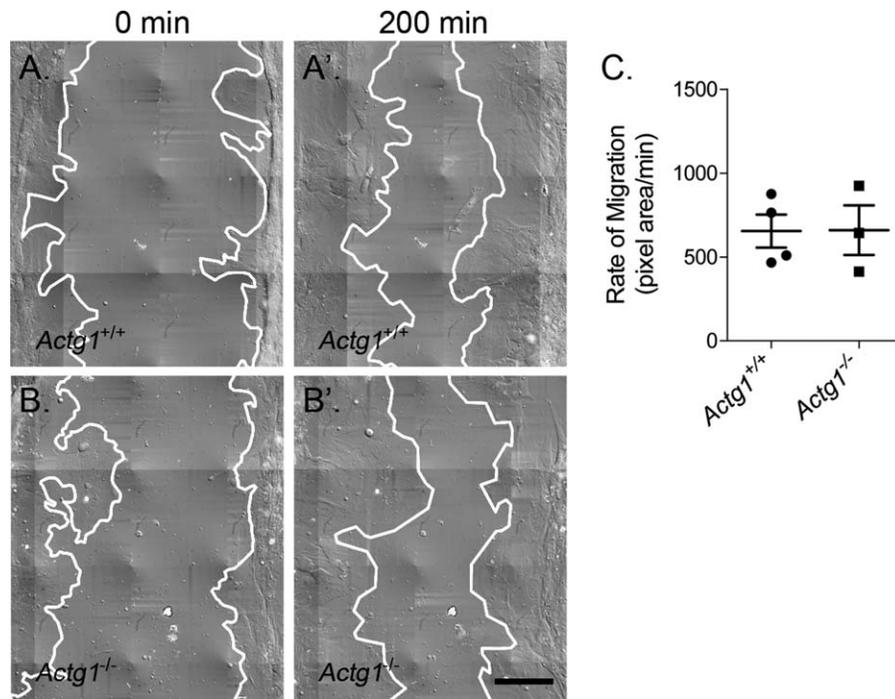
Fig. 5. Comparable rates of cell migration between wild-type and $Actg1^{-/-}$ MEFs. A–B: Still images from time-lapse video microscopy showing the wound edge in yellow at time 0 and 200 minutes from both $Actg1^{+/+}$ and $Actg1^{-/-}$ MEF cultures. **C:** Rates of cell migration were calculated as the change in wound area divided by the change in time ($n \geq 3$, mean ± s.e.m.). Scale bar: 100 μm.

maintained by upregulation of other actin isoforms, including the most closely related β_{cyto}-actin (Figs. 4a and 4b). These data are consistent with our previous findings that total actin expression was maintained in adult $Actg1^{+/-}$ and $Actg1^{-/-}$ animals [Belyantseva et al., 2009] and supports the existence of an actin feedback-regulatory mechanism [Leavitt et al., 1987; Ng et al., 1988; Lloyd et al., 1992].

We next determined whether the loss of γ_{cyto}-actin expression altered the ratio of globular (G)- to filamentous (F)-actin. It is well established that the G- to F-actin ratio is critical for proper regulation of the cytoarchitecture [Pollard and Borisy, 2003] and regulation of gene expression via serum response factor [Vartiainen et al., 2007; Busche et al., 2008]. Using a quantitative Western blot approach, we found that the G- to F-actin ratio in MEFs was maintained in the absence of γ_{cyto}-actin expression (Fig. 4c).

The fact that morphogenesis progresses normally in $Actg1^{-/-}$ embryos would suggest that γ_{cyto}-actin is not required for cell migration in vivo. To directly test the role of γ_{cyto}-actin during cell migration, however, we used an in vitro wound-healing assay. The rate of cell migration was comparable between $Actg1^{+/+}$ and $Actg1^{-/-}$ MEFs (Fig. 5), indicating that γ_{cyto}-actin is not necessary for proper cell migration.

Given the reduced size of $Actg1^{-/-}$ embryos, we analyzed growth properties of MEFs and found that $Actg1^{-/-}$ cells exhibited growth retardation compared to control cells (Fig. 6a). Comparable cell cycle profiles were observed between all genotypes (Figs. 6d and 6e), indicating that the growth defi-

ciency is not due to defects in the cell cycle. Furthermore, we did not observe a difference in the average cell diameter between wild-type and $Actg1^{-/-}$ MEFs (Fig. 6c), indicating that cell size was not altered by γ_{cyto}-actin ablation. The growth deficiency appears to be due to decreased cell survival, as cell viability was reduced in $Actg1^{-/-}$ MEFs compared to control cells (Fig. 6b). Decreased cell survival is at least in part due to increased apoptosis (Figs. 6f and 6g). As determined by an Annexin V assay, the percent of apoptotic cells increased from 5.0 ± 0.9 in wild-type MEFs to 8.6 ± 1.4 in $Actg1^{-/-}$ MEFs. While this increase is not statistically significant, the trend is consistent with the subtle growth deficiency observed in both $Actg1^{-/-}$ cells and animals.

Discussion

The high degree of conservation of small sequence differences between the cytoplasmic actins has suggested distinct requirements for the two isoforms. While γ_{cyto}-actin is not absolutely essential for viability [Belyantseva et al., 2009], we show that γ_{cyto}-actin clearly confers advantages during development, as $Actg1^{-/-}$ animals were smaller in size and exhibited a delay in the development of the cardiac outflow tract. Furthermore, most $Actg1^{-/-}$ mice died during the postnatal period, likely due to respiratory distress and subsequent cannibalization by the parents. In conjunction with our in vivo results, we observed reduced growth kinetics in $Actg1^{-/-}$ primary MEFs as a result of decreased cell survival. Taken together, our data
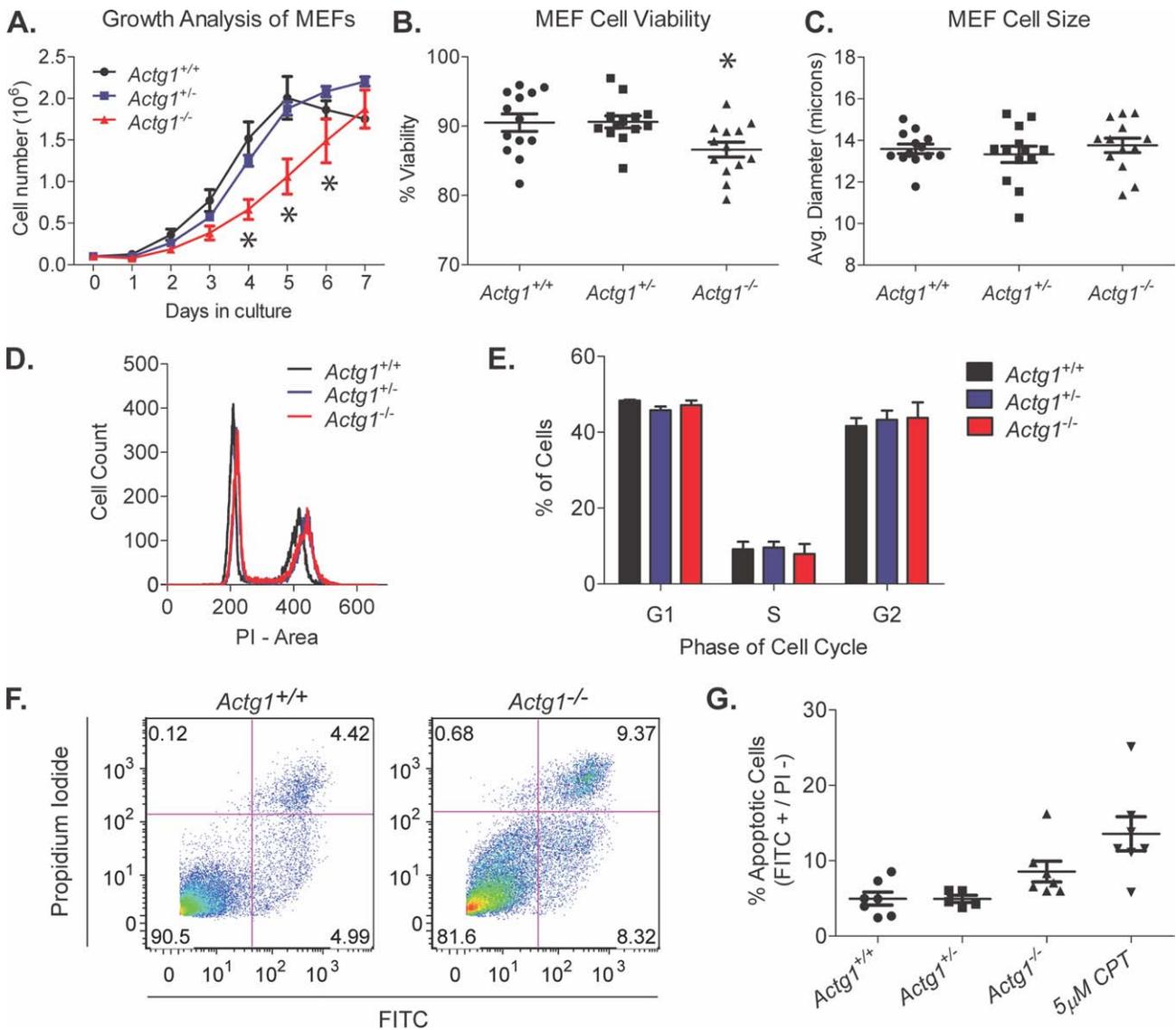
Fig. 6. Impaired growth due to decreased cell survival in *Actg1*$^{-/-}$ MEFs. A: Growth kinetics revealed impaired growth in *Actg1*$^{-/-}$ MEFs. $n = 4$ for each genotype; error bars represent s.e.m. Asterisks denote significant differences (two-way ANOVA, $P < 0.05$). **B**: Reduced cell viability in *Actg1*$^{-/-}$ MEFs as determined by an automated trypan blue exclusion assay ($n = 13$, mean ± s.e.m.). Asterisk denotes significant differences (one-way ANOVA, $P < 0.05$). **C**: Mean MEF cell size as determined by the ViCELL Series' automated contrast imaging and analysis ($n = 13$, mean ± s.e.m.). **D**: Representative cell cycle profiles. **E**: Mean percentage of cells in the G1, S, and G2 phases of the cell cycle ($n = 3$, mean ± s.e.m.). **F**: Dot plots from FITC-Annexin V flow cytometric analyses. The lower-right box represents early apoptotic cells (Annexin V-FITC Positive/ PI Negative) while the upper right box represents dead cells (Annexin V-FITC Positive/ PI Positive). **G**: Mean percentage of apoptotic cells, defined as FITC-positive and PI-negative ($n \geq 5$, mean ± s.e.m.). CPT, camptothecin.

illustrates that γ_{cyto}-actin provides a distinct advantage for growth and survival both in vitro and in vivo.

We provide evidence that increased apoptosis can at least partially account for the reduced cell survival of *Actg1*$^{-/-}$ MEFs. Many studies have demonstrated that actin plays a key role in the regulation of apoptosis [Franklin-Tong and Gourlay, 2008]. While actin has been linked to multiple stages of the apoptotic pathway, the precise mechanism by which actin regulates apoptosis remains elusive. A greater understanding of the exact function of actin in programmed cell death will be necessary to elucidate the mechanism whereby the loss of γ_{cyto}-actin leads to increased apoptosis.

Nonetheless, elevated levels of apoptosis provide a possible explanation for the reduced body size and delayed development in *Actg1*$^{-/-}$ embryos.

Until recently, β_{cyto}-actin was thought to be the actin isoform critical for cell motility. A range of studies have demonstrated that β_{cyto}-actin is enriched at the leading edge of migrating cells, while γ_{cyto}-actin is more uniformly distributed throughout the cell [Otey et al., 1986; Hoock et al., 1991; Hill and Gunning, 1993; Bassell et al., 1998; Micheva et al., 1998]. Furthermore, β_{cyto}-actin overexpression leads to increased areas of protrusion and cell migration [Peckham et al., 2001]. In contrast, Dugina et al. [2009] recently

reported that γ_{cyto}-actin is the predominate species at lamellipodial protrusions and that a modest decrease in γ_{cyto}-actin induced by siRNA knockdown caused severe cell migration defects. Our in vivo and in vitro results clearly demonstrate that γ_{cyto}-actin is not required for cell migration and is consistent with evidence that β_{cyto}-actin is the predominant isoform that drives cell migration.

It has long been thought that the strict evolutionary conservation of cytoplasmic actin coding sequences confers distinct and critical functions for β_{cyto} and γ_{cyto}-actin. We previously reported a progressive hearing loss in $Actg1^{-/-}$ adult mice [Belyantseva et al., 2009] that is similar to human patients with γ_{cyto}-actin point mutations [van Wijk et al., 2003; Zhu et al., 2003]. The fact that total actin levels are maintained in $Actg1^{-/-}$ mouse tissues [Belyantseva et al., 2009] and MEFs suggests that the phenotypes observed in $Actg1^{-/-}$ mice and cells are due to unique functions for γ_{cyto}-actin. The four amino acid differences between β_{cyto} and γ_{cyto}-actin are located at the N-terminus, where actin associated proteins are known to bind; however, there is limited evidence for actin isoform specific binding proteins [Shuster et al., 1996; Tzima et al., 2000]. Alternatively, differential expression patterns could account for the lack of complete compensation by alternate actin isoforms in $Actg1^{-/-}$ animals. The expression patterns of actin isoforms are known to be temporally and spatially regulated during development [McHugh et al., 1991]. A new mouse model will be necessary to test whether transgenic expression of β_{cyto}-actin, under the same regulatory control as γ_{cyto}-actin, can rescue the $Actg1^{-/-}$ phenotype.

Biochemical differences between β_{cyto} and γ_{cyto}-actin could also account for subtle cellular phenotypes. Bergeron et al. (2010) recently reported that γ_{cyto}-actin filaments are less dynamic than β_{cyto}-actin filaments, with γ_{cyto}-actin polymerizing more slowly and exhibiting enhanced filament stability. These intrinsic biochemical differences likely contribute to the distinct requirements of the two cytoplasmic actins.

Acknowledgments

References

Anderson RH, Webb S, Brown NA, Lamers W, Moorman A. 2003. Development of the heart: (3) formation of the ventricular outflow tracts, arterial valves, and intrapericardial arterial trunks. Heart 89(9):1110–1118.

Bassell GJ, Zhang H, Byrd AL, Femino AM, Singer RH, Taneja KL, Lifshitz LM, Herman IM, Kosik KS. 1998. Sorting of beta-actin mRNA and protein to neurites and growth cones in culture. J Neurosci 18(1):251–265.

Belyantseva IA, Perrin BJ, Sonnemann KJ, Zhu M, Stepanyan R, McGee J, Frolenkov GI, Walsh EJ, Friderici KH, Friedman TB, Ervasti JM. 2009. Gamma-actin is required for cytoskeletal maintenance but not development. Proc Natl Acad Sci USA 106(24):9703–9708.

Bergeron SE, Zhu M, Thiem SM, Friderici KH, Rubenstein PA. 2010. Ion-dependent polymerization differences between mammalian beta- and gamma-nonmuscle actin isoforms. J Biol Chem 285(21):16087–16095.

Busche S, Descot A, Julien S, Genth H, Posern G. 2008. Epithelial cell-cell contacts regulate SRF-mediated transcription via Rac-actin-MAL signalling. J Cell Sci 121 (Part 7):1025–1035.

Copp AJ, Greene ND, Murdoch JN. 2003. The genetic basis of mammalian neurulation. Nat Rev Genet 4(10):784–793.

Dugina V, Zwaenepoel I, Gabbiani G, Clement S, Chaponnier C. 2009. Beta and gamma-cytoplasmic actins display distinct distribution and functional diversity. J Cell Sci 122 (Part 16):2980–2988.

Franklin-Tong VE, Gourlay CW. 2008. A role for actin in regulating apoptosis/programmed cell death: evidence spanning yeast, plants and animals. Biochem J 413(3):389–404.

Furness DN, Katori Y, Mahendrasingam S, Hackney CM. 2005. Differential distribution of beta- and gamma-actin in guinea-pig cochlear sensory and supporting cells. Hear Res 207(1–2):22–34.

Harborth J, Elbashir SM, Bechert K, Tuschl T, Weber K. 2001. Identification of essential genes in cultured mammalian cells using small interfering RNAs. J Cell Sci 114 (Part 24):4557–4565.

Hill MA, Gunning P. 1993. Beta and gamma actin mRNAs are differentially located within myoblasts. J Cell Biol 122(4):825–832.

Hoock TC, Newcomb PM, Herman IM. 1991. Beta actin and its mRNA are localized at the plasma membrane and the regions of moving cytoplasm during the cellular response to injury. J Cell Biol 112(4):653–664.

Jacinto A, Baum B. 2003. Actin in development. Mech Dev 120(11): 1337–1349.

Kaufman MH. 1992. The Atlas of Mouse Development. London: Elsevier Academic Press.

Leavitt J, Ng SY, Aebi U, Varma M, Latter G, Burbeck S, Kedes L, Gunning P. 1987. Expression of transfected mutant beta-actin genes: alterations of cell morphology and evidence for autoregulation in actin pools. Mol Cell Biol 7(7):2457–2466.

Lloyd C, Schevzov G, Gunning P. 1992. Transfection of nonmuscle beta- and gamma-actin genes into myoblasts elicits different feedback regulatory responses from endogenous actin genes. J Cell Biol 117(4):787–797.

Marston DJ, Goldstein B. 2006. Actin-based forces driving embryonic morphogenesis in Caenorhabditis elegans. Curr Opin Genet Dev 16(4): 392–398.

McHugh KM, Crawford K, Lessard JL. 1991. A comprehensive analysis of the developmental and tissue-specific expression of the isoactin multigene family in the rat. Dev Biol 148(2):442–458.

Micheva KD, Vallee A, Beaulieu C, Herman IM, Leclerc N. 1998. beta-Actin is confined to structures having high capacity of remodelling in developing and adult rat cerebellum. Eur J Neurosci 10(12):3785–3798.

Ng SY, Erba H, Latter G, Kedes L, Leavitt J. 1988. Modulation of microfilament protein composition by transfected cytoskeletal actin genes. Mol Cell Biol 8(4):1790–1794.

Otey CA, Kalnoski MH, Lessard JL, Bulinski JC. 1986. Immunolocalization of the gamma isoform of nonmuscle actin in cultured cells. J Cell Biol 102(5):1726–1737.

Peckham M, Miller G, Wells C, Zicha D, Dunn GA. 2001. Specific changes to the mechanism of cell locomotion induced by overexpression of beta-actin. J Cell Sci 114 (Part 7):1367–1377.

Pollard TD, Borisy GG. 2003. Cellular motility driven by assembly and disassembly of actin filaments. Cell 112(4):453–465.

Rubenstein PA. 1990. The functional importance of multiple actin isoforms. Bioessays 12(7):309–315.

Shawlot W, Deng JM, Fohn LE, Behringer RR. 1998. Restricted beta-galactosidase expression of a hygromycin-lacZ gene targeted to the beta-actin locus and embryonic lethality of beta-actin mutant mice. Transgenic Res 7(2):95–103.

Shmerling D, Danzer CP, Mao X, Boisclair J, Haffner M, Lemaistre M, Schuler V, Kaeslin E, Korn R, Burki K, Ledermann B, Kinzel B, Muller M. 2005. Strong and ubiquitous expression of transgenes targeted into the beta-actin locus by Cre/lox cassette replacement. Genesis 42(4):229–235.

Shuster CB, Lin AY, Nayak R, Herman IM. 1996. Beta cap73: a novel beta actin-specific binding protein. Cell Motil Cytoskeleton 35(3): 175–187.

Sonnemann KJ, Fitzsimons DP, Patel JR, Liu Y, Schneider MF, Moss RL, Ervasti JM. 2006. Cytoplasmic gamma-actin is not required for skeletal muscle development but its absence leads to a progressive myopathy. Dev Cell 11(3):387–397.

Tzima E, Trotter PJ, Orchard MA, Walker JH. 2000. Annexin V relocates to the platelet cytoskeleton upon activation and binds to a specific isoform of actin. Eur J Biochem 267(15):4720–4730.

van Wijk E, Krieger E, Kemperman MH, De Leenheer EM, Huygen PL, Cremers CW, Cremers FP, Kremer H. 2003. A mutation in the gamma actin 1 (ACTG1) gene causes autosomal dominant hearing loss (DFNA20/26). J Med Genet 40(12):879–884.

Vartiainen MK, Guettler S, Larijani B, Treisman R. 2007. Nuclear actin regulates dynamic subcellular localization and activity of the SRF cofactor MAL. Science 316(5832):1749–1752.

Yao X, Chaponnier C, Gabbiani G, Forte JG. 1995. Polarized distribution of actin isoforms in gastric parietal cells. Mol Biol Cell 6(5): 541–557.

Zhu M, Yang T, Wei S, DeWan AT, Morell RJ, Elfenbein JL, Fisher RA, Leal SM, Smith RJ, Friderici KH. 2003. Mutations in the gamma-actin gene (ACTG1) are associated with dominant progressive deafness (DFNA20/26). Am J Hum Genet 73(5):1082–1091.